IEEE Access
Multidisciplinary | Rapid Review | Open Access Journal

Received September 17, 2020, accepted September 25, 2020, date of publication September 29, 2020,
date of current version October 12, 2020.

Digital Object Identifier 10.1109/ACCESS.2020.3027623

An Intelligent Deep Learning-Based Direction-of-Arrival Estimation Scheme Using Spherical Antenna Array With Unknown Mutual Coupling

OLUWOLE JOHN FAMORIJI[1], (Member, IEEE), OLUDARE Y. OGUNDEPO[2], AND XIAOKANG QI[3], (Member, IEEE)

[1]Ocean College, Institute of Marine Electronic and Intelligent System, Zhejiang University, Zhoushan 316021, China
[2]Department of Electrical and Electronic Engineering, Federal University of Petroleum Resources, Effurun, Warri 562101, Nigeria
[3]Laboratory of Applied Research on Electromagnetics (ARE), Zhejiang University, Hangzhou 310027, China

Corresponding authors: Xiaokang Qi (qixk@zju.edu.cn) and Oluwole John Famoriji (famoriji@mail.ustc.edu.cn)

This work was supported in part by the Fundamental Research Funds for the Central Universities, and in part by the National Natural Science Foundation of China (NSFC) under Grant 61674128 and Grant 61731019.

ABSTRACT Spherical antenna array (SAA) has become highly attractive where hemispherical scan coverage is required as it can provide uniform directivity in all the scan directions. Various direction-of-arrival (DoA) estimation methods suffer from different problems, such as low accuracies in mismatched conditions, high computational complexity and poor estimation in a harsh environment. Another critical concern is mutual coupling (MC) characteristics between the array elements. These problems affect the quality of the navigation signal in harsh environments. This paper presents a robust DoA estimation and mutual coupling compensation technique based on convolutional neural network (CNN) for Spherical Array. Spherical harmonic decomposition (SHD) is used to facilitate feature extraction in two sets, which contains different features about the elevation and azimuth of the source for DoA estimation. The features serve as input to the learning technique for separate estimation of elevation and azimuth, which consequently reduce computational complexity as against the joint estimation of DoA. Learning methods for DoA estimation with few frames and dense search grids within the spherical array configuration are presented. To solve the MC error, the DoA estimation scheme is also used to obtain accurate spectrum peak in the multipath scenario with unknown MC and sharper spectrum peak via the unique structure of the MC matrix and spatial smoothing algorithms. In all, experimental results, which is the ground truth to test any procedure, show the effectiveness, validity, and potential practical application of the proposed technique.

INDEX TERMS Spherical arrays, DoA estimation, mutual coupling, learning method, spherical harmonic decomposition, CNN, smoothing algorithm.

I. INTRODUCTION

A. INCITATION AND MOTIVATION

Direction-of-arrival (DoA) estimation is a popular topic in various electromagnetic related fields of study, which finds applications in military surveillance, radar, sonar, and mobile communication systems [1]–[3]. Understanding the DoAs of incoming signals on the receiving antenna can be effectively used to localize the positions of corresponding sources. It facilitates adaptive beamforming of the receiving pattern to improve the sensitivity of the system towards the desired directions of signals and mitigates undesirable interferences. Therefore, DoA estimation of electromagnetic (EM) waves impinging onto an antenna array is very important. Also, there is an explosive development of wireless applications in state-of-the-art mobile terminals, automobiles, and laptops. In order to fulfill the requirements of the growing applications, particular number of antennas are installed on those systems. The average distance between the antennas is becoming smaller, which leads to strong mutual coupling and poor radiation performance and impedance matching [4], [5].

Spherical antenna array (SAA) configuration is useful in obtaining an array with isotropic characteristics. There is also a spherical phased antenna array, which is widely used

The associate editor coordinating the review of this manuscript and approving it for publication was Wei Wang.

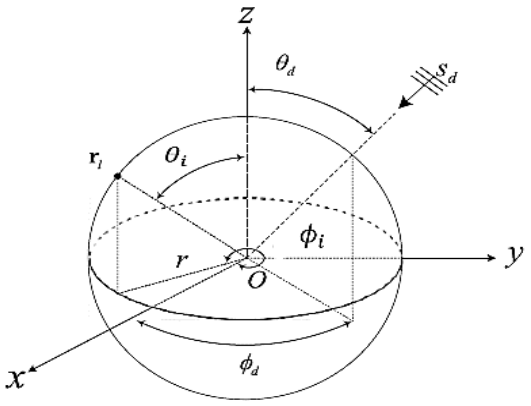

FIGURE 1. Spherical array geometry system for localization.

spacecraft and satellite communication. The electronic beam scanning by the phased antenna array remains a better choice because it gives a hemispherical scan and almost uniformly distributed gain [6], [7]. Another major advantage of SAA configuration is its 3-Dimensional symmetry, which is an advantage in spatial analysis of signals. The geometry and size usually provide the directivity and degree of beam scanning in elevation and azimuth needed from the array. The Linear array, which scans in one axis, and planar array, which scans in x- and y-axes are acceptable for a bounded scan demand of 60-70^0 [7]. The projected apertures of these arrays fall by the cosine factor of the scan angle. The array directivity dropped in the case of a big scan angle. For larger steering capacity, a multifold planar configuration, or in a general form, an SAA is preferred [6]. Hence, the DoA estimation and mutual coupling calibration algorithm for SAA becomes necessary.

B. CONVENTIONAL CONFIGURATION OF SAA

The geometry and basic configuration of SAA is as depicted in Figure 1, where θ_i and ϕ_i represent the elevation and azimuth of the ith element, respectively. θ_d and ϕ_d denote the elevation and azimuth of the incident plane wave, respectively, while s_d is the source signal. The radiating antenna elements are evenly distributed over a sphere of radius r. The traditional distributions of antenna array on a geodesic sphere depend on one of the 13 Archimedean solids or the 5 platonic solids [3], [6]. Here, the fundamental merit is that all elements encounter the same neighborhood. Conversely, other various distributions could be figured out based on beam scanning requirements and the number of antenna elements under use. For icosahedron distribution along the elevation axis, the elements are organized in circular bands. In each circular band, the locations in azimuth are estimated. Furthermore, any far-field observation point can be defined as $p(r, \theta, \phi)$.

The SAA is in the active mode, where each element is supplied with an amplifier. To receive a beampattern in a specific direction (θ_0, ϕ_0), the elements lying within the predetermined cone angle around the beam direction are in active mode. These elements are activated using accurate phases estimated from the equations in [6] and [7].

C. RELATED WORKS

Various methods for estimation of DoA within the context of linear and planar arrays have been reported earlier. Due to the advantages of SAA, many methods utilizing SAA are currently being considered. For instance, multiple signal classification (MUSIC) and estimation of signal parameters via rotational invariance techniques (ESPRIT) have been considered in the spherical harmonic domain [8]–[10], and a detailed comparison is reported in [10]. It is important to note that these methods are used for reflected signals localization as against the DoAs of sources. Spherical harmonic MUSIC (SH-MUSIC) is proven robust in harsh environments. Learning techniques have also been reported whereby the signal features extracted from measurements are fed into the neural network that has been trained [11]–[14]. Other DoA estimation methods in the spherical harmonic domain are: generalized cross-correlation (GCC), steered response power with phase transform, and the minimum variance distortionless response [14].

Furthermore, deep learning approaches have been used to estimate DoA and solve source localization problem with microphone arrays [15]–[19]. Very challenging cases with wideband signals [18], [19], dynamic acoustic signal [15] and reverberation effects [16], [17] were considered. Also, a framework basedon deep neural network that addresses DoA estimation problem has been proposed in [20]. The technique exhibits good adaptation to array imperfections and enhance enhance generalization to unseen cases. Kase *et al.* [21] employed deep learning to estimate DoA and evaluates the performance in the for two narrowband signals incident on linear array. Deep neural network shows appreciable estimation accuracy. The deep learning formulated for a particular case exhibits very high success rate in the same case [21]. Wan *et al.* [22] proposed a deep learning based autonomous vehicle super resolution DoA estimation for safety driving. Deep learning architecture was implemented to learn the nonlinear feature from the DoAs of autonomous vehicles and the received data was collected by reconfigurable intelligent surface or massive MIMO (multiple input multiple output). The parameters of DoA and polarization were estimated based on the architecture (SBLNet) with relatively low computational complexity. Similarly, Wen *et al.* [23] proposed auxiliary vehicle positioning based on a robust estimation with unknown mutual coupling. An auxiliary positioning architecture was proposed to estimate DoA from landmarks, such as wireless access points, utilizing sensor array in the vehicle. The proposed algorithm obtains robust self–localization with existing vehicle ad hoc networks and used with other positioning systems to give a safety environment.

Elbir [24] developed a data transformation technique for the estimation of DoA with 3-D antenna arrays with mutual coupling effect. The technique is based on decomposition of mutual coupling matrix as a function of the unknown distinct coefficient of mutual coupling. This technique shows good performance and high accuracy with 3-D array structures.

Therefore, in present literature, there are several DoA eatimation methods with unknown mutual coupling for different array geometries. Specifically, there has been much focus on DoA estimation using linear, circular, and rectangular antenna arrays, with little or no effort so far on SAA.

The generally established mutual coupling correction approaches for antenna arrays are classified into two classes. The first class deal with the compensation of or calibration of mutual coupling in decoupled network design and antenna array design. In the second class, the mutual coupling is corrected by solving the mutual coupling matrix (MCM) via array signal processing and analysis of electromagnetics (EM) [25]. The implementation of the first approach is more challenging in engineering. The approach is based on the analysis of EM, such as the S-scattering parameter technique, and open-circuit voltage technique are only applied to transmit mode arrays. Full-wave approach and reception of the mutual impedance approach require larger measurement data, and the steps involved are complicated. From the perspective of array signal processing, the blind calibration approach uses MCM banded symmetric Toeplitz structure. Mutual coupling calibration can be achieved using matrix transformation or separation of mutual coupling coefficient. The blind calibration approach, when combined with the estimation algorithm, simultaneously estimates mutual coupling parameters and DoAs [26].

D. PROBLEM

At least one of the following demerits limits the DoA estimation methods mentioned above: adaptation problem to electromagnetic environments, computational complexity, poor estimation in harsh environments, inaccuracies under mismatched situations.

Learning methods have been successfully used in DoA estimation, where the feature is extracted from measurements and passed to a neural network that has been trained for DoA feature mapping [12]–[14]. However, learning methods with dense DoA search grids and with a small number of frames within the spherical array configurations have not been dealt with.

Disjointed estimation of DoA via separate finding of azimuth and elevation angles reduces computational complexity, as reported in [27]–[29]. However, this has not been examined in the spherical domain. The decomposition of signal pressure at the elements into separate functions of elevation and azimuth of the source can be facilitated via spherical harmonic decomposition (SHD) [30].

In order to fulfill the requirements of the growing applications, particular number of antennas are installed on systems. The average distance between the antennas is becoming smaller, which leads to strong mutual coupling and poor radiation performance, and impedance matching.

E. CONTRIBUTIONS

In contrast to previous works, the main innovation and contributions of this work are as follows. At first, we propose a feature extraction technique using SHD in far-field wave propagation. Secondly, a convolutional neural network (CNN) scheme that uses the extracted features is developed for adequate estimation of DoA. Thirdly, we extended the proposed method to a dense DoA search grid and lastly, a DoA correction algorithm for joint mutual coupling error is adapted towards successful calibration of mutual coupling in SAAs.

F. ORGANIZATION

The rest part of this paper is organized as follows. The Signal model that is based on spherical harmonics is presented in Section II. Section III explains how the magnitude and phase features extraction are done via SHD. The CNN architecture and corresponding features in conjunction with their nature of training for estimation of DoA are presented in Section IV. The DoA correction algorithm for joint mutual coupling error and calibration is given in Section V. The procedure of the proposed DoA estimation and mutual coupling calibration is provided in Section VI. Section VII presents a performance evaluation of the proposed scheme and comparison with state-of-the-art via experiment. Conclusions are drawn in Section VIII.

II. SIGNAL MODEL

Let us consider far-field source at a position $\boldsymbol{r}_s = (r_s, \theta_s, \phi_s)$, where r_s denotes the radial distance while (θ_s, ϕ_s) represents the direction in the spherical coordinates [31]. Assuming an SAA is positioned with its origin at the same origin point of a coordinate system and its antenna elements at $\boldsymbol{r}_u = (r_u, \theta_u, \phi_u)$, where $u = 1, 2, 3 \ldots M$. Also, r represents the radius of SAA, and M denotes the number of elements in the SAA. The vector of the wave that corresponds to the source is $\boldsymbol{k} = (k, \theta_s, \phi_s)$ in the spherical coordinate system where $k = 2\pi f / c$ is the wavenumber. c denotes the speed of the propagating wave. With spherical harmonics (SH), signal pressure at point $\boldsymbol{r} = (r, \theta, \phi)$ of a particular plane wave using variables separation method [30] can be expressed as

$$p(k, \boldsymbol{r}) = e^{i\boldsymbol{k}.\boldsymbol{r}} = \sum_{n=0}^{N} \sum_{m=-n}^{n} b_n(kr) \left[Y_n^m(\theta_s, \phi_s)\right]^* Y_n^m(\theta, \phi) \quad (1)$$

where N is the order of SAA, and $[.]^*$ denotes the complex conjugate. The SH order truncation in spatial sampling is made to prevent the problem of aliasing that is similar to that of the limited bandwidth in time domain sampling [32]. $b_n(kr)$ is known as mode strength expressed as

$$b_n(kr) = 4\pi i^n \begin{cases} j_n(kr) & \textit{Open sphere} \\ j_n(kr) - \dfrac{j_n'(kr)}{h_n'(kr)} h_n(kr) & \textit{rigid sphere} \end{cases} \quad (2)$$

where j_n, *and* h_n represent the Bessel function of the first kind and Hankel function of the second kind, respectively, while j_n'

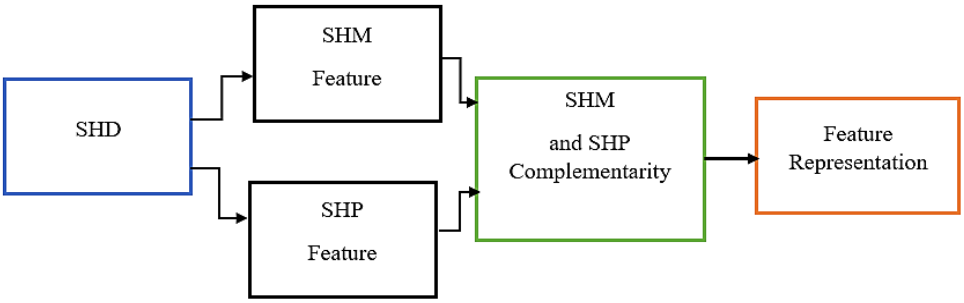

FIGURE 2. Feature extraction process for DoA estimation. SHM is the acronym for spherical harmonic magnitude while SHP is spherical harmonic phase.

and h_n' are the respective derivatives. $Y_n^m(\theta, \phi)$ is the SH basis functions expressed as

$$Y_n^m(\theta, \phi) = \sqrt{\frac{2n+1\,(\text{n-m})!}{4\pi\,(n+m)!}} P_n^m(cos\theta) e^{-im\phi} \tag{3}$$

where P_n^m denotes the Legendre function of degree m and order n. The matrix formulation of Eqn. (1) can be written for a signal strength $s(k)$ as

$$\boldsymbol{p}(k) = \boldsymbol{Y}(\Omega)\,\boldsymbol{B}(kr)\,\boldsymbol{y}^H(\theta_s, \phi_s)\,s(k) + \boldsymbol{z}(k) \tag{4}$$

where

$$\boldsymbol{p}(k) = [p(k, \boldsymbol{r}_1)\,p(k, \boldsymbol{r}_2)\ldots p(k, \boldsymbol{r}_M)]^T \tag{5}$$

$$\boldsymbol{B}(kr) = diag(b_0(kr)\,b_1(kr)\ldots b_N(kr)) \tag{6}$$

$[.]^{\mathrm{T}}$ represents transpose while $[.]^{\mathrm{H}}$ is the conjugate transpose. The SH matrix of the antenna element positions, $\boldsymbol{Y}(\Omega)$, can be expressed as

$$\boldsymbol{Y}(\Omega) = \left[\boldsymbol{y}^T(\theta_1, \phi_1)\,\boldsymbol{y}^T(\theta_2, \phi_2)\ldots\boldsymbol{y}^T(\theta_M, \phi_M)\right]^T \tag{7}$$

where

$$\boldsymbol{y}(\theta, \phi) = \left[Y_0^0(\theta, \phi)\,Y_1^{-1}(\theta, \phi)\ldots Y_N^N(\theta, \phi)\right] \tag{8}$$

and the noise vector $\boldsymbol{z}(k)$ is given as

$$\boldsymbol{z}(k) = [z_1(k)\,z_2(k)\ldots z_M(k)]^T \tag{9}$$

Spatial domain transformation to SH domain is defined as

$$\boldsymbol{P}_{nm}(k) = \boldsymbol{Y}^H(\Omega)\,\boldsymbol{p}(k) \tag{10}$$

Applying the principle of orthogonality for nearly uniform or uniform sampling, the SH coefficients are then obtainable from Eqn. (4) as

$$\boldsymbol{P}_{nm}(k) = \boldsymbol{B}(kr)\,\boldsymbol{y}^H(\theta_s, \phi_s)\,s(k) + \boldsymbol{z}_{nm}(k) \tag{11}$$

where

$$\boldsymbol{z}_{nm}(k) = \boldsymbol{Y}^H(\Omega)\,\boldsymbol{z}(k)$$

For SAA, we can multiply Eqn. (11) by $\boldsymbol{B}^{-1}(kr)$ to give

$$\boldsymbol{q}_{nm}(k) = \boldsymbol{y}^H(\theta_s, \phi_s)\,s(k) + \tilde{\boldsymbol{z}}_{nm}(k) \tag{12}$$

where

$$\boldsymbol{q}_{nm}(k) = \boldsymbol{B}^{-1}(kr)\,\boldsymbol{P}_{nm}(k),$$
$$\tilde{\boldsymbol{z}}_{nm}(k) = \boldsymbol{B}^{-1}(kr)\,\boldsymbol{z}_{nm}(k).$$

To avoid aliasing problem, kr is set to $n \leq kr \leq N$. For time-domain analysis, it is preferable to consider the signals in short time Fourier transform (STFT) domain in conjunction with the transfer function (multiplicative). Therefore, the signal model of Eqn. (12) results to

$$\boldsymbol{q}_{nm}(\rho, \varpi) = \boldsymbol{y}^H(\theta_s, \phi_s)\,s(\rho, \varpi) + \tilde{\boldsymbol{z}}_{nm}(\rho, \varpi) \tag{13}$$

where ρ and ϖ are the frame number index and frequency bin from STFT. The first component of right hand side in Eqn. (13) is the target (termed $\boldsymbol{q}_{nm}^t(\rho, \varpi)$) while the second one (termed $\boldsymbol{q}_{nm}^n(\rho, \varpi)$) is the noise component of $\boldsymbol{q}_{nm}$.

III. USING SHD FOR FEATURE EXTRACTION TOWARDS DoA ESTIMATION

The process of using SHD to extract the magnitude and phase features is presented in this section. The procedure is as summarized in Figure 2. Each block is explained below.

A. SHD

SH facilitates the expression of the solution of wave equation using a variable separation approach [20] as

$$p(\boldsymbol{r}, t) = F(\mathrm{r})\,\varphi(\theta)\,\Psi(\phi)Q(t) \tag{14}$$

where θ and ϕ are the elevation and azimuth angles, respectively. The $p(\boldsymbol{r}, t)$ is the pressure of signal expressed in time and space. Eqn. (14) is solved by

$$\begin{aligned} R(\mathrm{r}) &= j_n(kr) \\ \Psi(\phi) &= e^{im\phi} \\ \varphi(\theta) &= P_n^m(cos\theta) \\ Q(t) &= e^{i\omega t} \end{aligned} \tag{15}$$

The SHD given by Eqn. (15) forms the basis of the proposed SHM (spherical harmonic magnitude) and SHP (spherical harmonic phase) based features.

B. INVARIANCE IN SH DOMAIN

From the SH domain of the signal model in Eqn. (13), the target component of the coefficient of SH is defined as

$$\boldsymbol{q}_{nm}^{t}(\rho,\varpi)=[Y_n^m(\theta_s,\phi_s)]^* s(\rho,\varpi) \tag{16}$$

The component of zero-order and zero degree $q_{00}^{t}(\rho,\varpi)$ is given as

$$q_{00}^{t}(\rho,\varpi)=[Y_0^0(\theta_s,\phi_s)]^* s(\rho,\varpi)=\frac{s(\rho,\varpi)}{\sqrt{4\pi}} \tag{17}$$

It becomes obvious that $q_{00}^{t}(\rho,\varpi)$ does not depend on the source DoA and it indicates $s(\rho,\varpi)$ [33]. We used the signal dependence property of $q_{00}^{t}(\rho,\varpi)$ in obtaining the signal invariant features.

C. SHM FEATURES

In Eqn. (13), the magnitude of SH coefficients $q_{nm}^{t}(\rho,\varpi)$ can be expressed as

$$\begin{aligned}\left|q_{nm}^{t}(\rho,\varpi)\right| &= \left|Y_n^m(\theta_s,\phi_s)\right|\,|s(\rho,\varpi)|\\ &= \xi_{nm}\left|P_n^m(cos\theta_s)\right|\,|s(\rho,\varpi)|\end{aligned} \tag{18}$$

and

$$\xi_{nm}=\sqrt{\frac{2n+1}{4\pi}\frac{(\text{n-m})!}{(n+m)!}} \tag{19}$$

It is seen how the magnitude of SH coefficients depend on $s(\rho,\varpi)$ and θ_s. The signal dependence concept in Eqn. (17) is applicable here, the magnitude is considered independent on the signal strength and is given as

$$\begin{aligned}\hat{q}_{nm}^{t}(\rho,\varpi) &= \frac{\left|q_{nm}^{t}(\rho,\varpi)\right|}{\left|q_{00}^{t}(\rho,\varpi)\right|}\\ &= \sqrt{4\pi}\xi_{nm}\left|P_n^m(cos\theta_s)\right|\end{aligned} \tag{20}$$

Therefore, the SHM features contain only the elevation information and with no information about the azimuth.

D. SHP FEATURES

From Eqn. (13) the phase of the SH coefficients $q_{nm}^{t}(\rho,\varpi)$ can be expressed as

$$\begin{aligned}\angle q_{nm}^{t}(\rho,\varpi) &= \angle(Y_n^m(\theta_s,\phi_s)\,s(\rho,\varpi)\\ &= \angle P_n^m(cos\theta_s)+m\phi_s+\angle s(\rho,\varpi)\end{aligned} \tag{21}$$

Conversely, $P_n^m(.)$ are functions with real value that add π or 0 to phase depending on the nature of the function, whether it is negative or positive. Therefore, Eqn. (21) is now

$$\angle q_{nm}^{t}(\rho,\varpi)=\pi I_{nm}(\theta_s)+m\phi_s+\angle s(\rho,\varpi) \tag{22}$$

where

$$I_{nm}(\theta)=\begin{cases}1 & if\ P_n^m(cos\theta)<0\\ 0 & if\ P_n^m(cos\theta)\geq 0\end{cases} \tag{23}$$

From Eqn. (22), it can be seen that the phase of $q_{nm}^{t}(\rho,\varpi)$ equally depends on $s(\rho,\varpi)$. In Eqn. (17) the signal dependence concept can be used for the features here and make it independent of the phase associated with $q_{nm}^{t}(\rho,\varpi)$ as

$$\begin{aligned}\angle\hat{q}_{nm}^{t}(\rho,\varpi) &= \angle q_{nm}^{t}(\rho,\varpi)-\angle q_{00}^{t}(\rho,\varpi)\\ &= \pi I_{nm}(\theta_s)+m\phi_s\end{aligned} \tag{24}$$

Therefore, it is observed that the SHP features contain the information of the source about the elevation and azimuth.

E. SHM AND SHP FEATURES COMPLEMENTARITY

It becomes clear that both SHP and SHM have complementarity DoA information. The combined version of SHP and SHM, called SHPM, can be applied for the estimation of DoA. This is needed because the SHP has information of the source about the elevation and azimuth, while SHM contains information about the elevation alone.

F. REPRESENTATION OF FEATURE

The feature taken from the measurements contains both target component and noise. They are fed into a learning scheme that is described in the next section. The matrix of the feature has $(N+1)^2$ various SH at the number of frequency bins N_F. Since, $\hat{q}_{00}^{t}(k)$ carries no DoA information, the SHM feature has a dimension of $((N+1)^2-1)\times N_F$. For the SHP feature, the phase of $\hat{q}_{nm}(k)$ serves as the input under equal 0 and 2π conditions. Therefore, sine and cosine characteristic of phase is given as input [34] leading to $2((N+1)^2-1)\times N_F$ dimensions. For SHPM features, both SHP and SHM features are concatenated in SH dimension, the dimension of the feature is $3((N+1)^2-1)\times N_F$. For instance, if $N=2$ and $N_F=57$, the dimension of SHP is 14×57, while that of SHPM is 21×57. The procedure involved in DoA estimation using the proposed SH feature as input is presented and explained in the next section.

IV. DEEP LEARNING SCHEME FOR DoA ESTIMATION

In this section, a convolutional neural network scheme is presented for the estimation of DoA using the SH feature as the input. Noise, reflection etc. impair the SH features in practice. However, a learning method is possible for the utilization of these features towards the estimation of DoAs.

A. DoA ESTIMATION VIA CNN SCHEME

For a given feature ζ having the knowledge of DoA, the posteriori probability $P_r((\theta,\phi)|\zeta)$ can be calculated by CNN that has been trained using appropriate labels and features. The joint estimation of DoA via the rule of the maximum posteriori probability (MAP) is

$$(\hat{\theta}_s,\hat{\phi}_s)=\arg\max_{(\theta,\phi)}\Pr((\theta,\phi)|\zeta) \tag{25}$$

Applying variables separation for SHD, elevation and azimuth are separately estimated by

$$\hat{\theta}_s=\arg\max_{\theta}\Pr(\theta|\zeta)$$

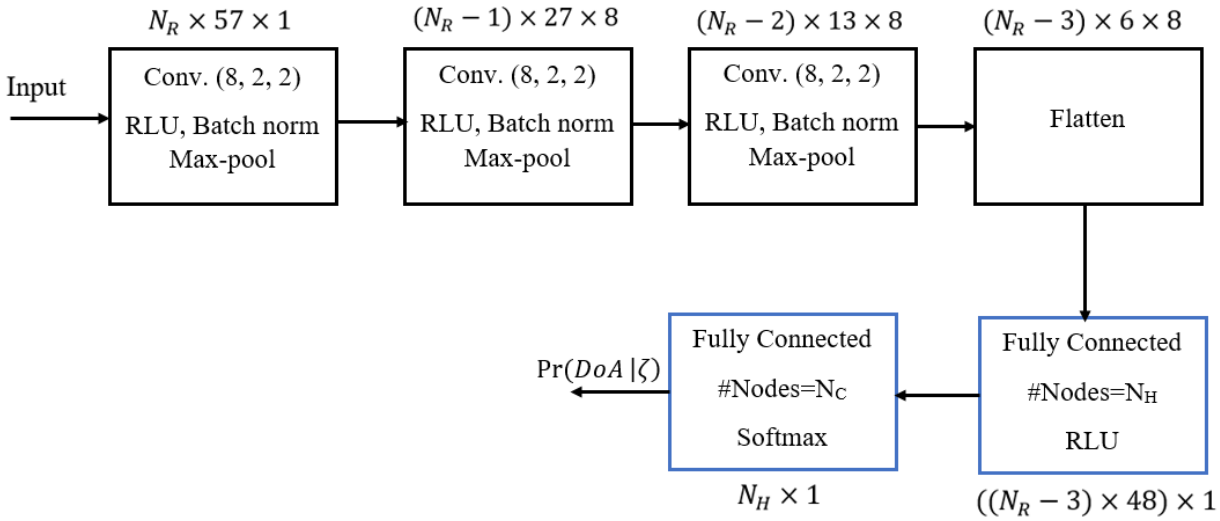

FIGURE 3. Architecture of the CNN scheme using SH feature for DoA estimation. *Conv* (a, b, c) means the size of the convolution filter (b, c) with the number of output filters a. N_H is the number of nodes in the first fully connected layer while N_C is the number of classes.

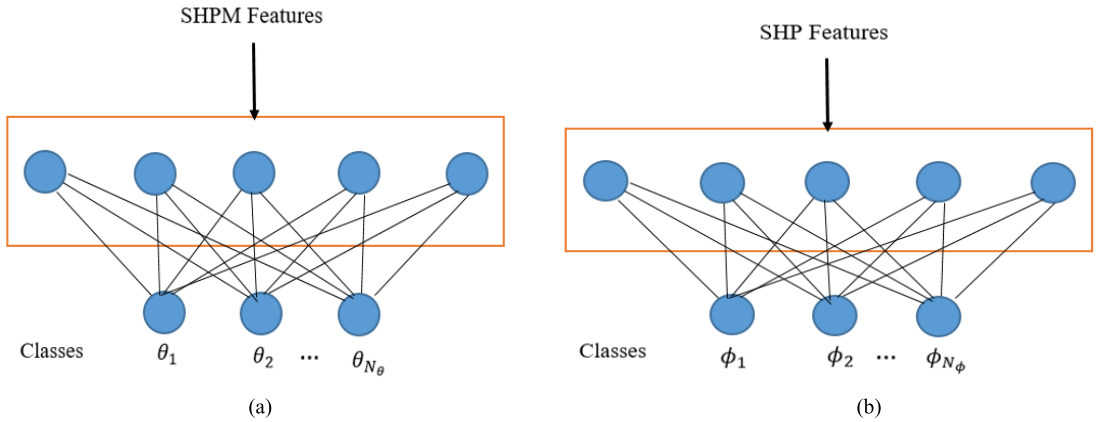

FIGURE 4. DoA estimation with CNN. (a) with SHPM features as input for elevation estimation (b) with SHP features as input for azimuth estimation. N_θ and N_ϕ are the number of classes.

$$\hat{\phi}_s = \arg\max_{\phi} \Pr(\phi|\zeta) \tag{26}$$

Note: $\Pr(\theta|\zeta)$ and $\Pr(\phi|\zeta)$ are computed from different learning methods. Various SH features and the information contained in them give the estimate of DoA using SHPM and SHP features for the estimation of θ and ϕ, respectively. Based on the reports in the literature, it is better to estimate DoA by the problem of classification instead of regression [16]. Therefore, two CNNs are needed since there is a need for two classifications. The first CNN performs the classification of the input feature as azimuth classes ϕ_j where $j\epsilon\{1, 2, 3, \ldots, N_\phi\}$ and the second CNN classifies into elevation θ_j where $j\epsilon\{1, 2, 3, \ldots, N_\theta\}$. This approach reduces the complexity of joint estimation.

B. THE ARCHITECTURE OF THE CNN

Here, the CNN calculates a function mapping the input feature to the DoA class. The CNN is made up of convolutional layers and fully connected layers. The architecture of CNN is as presented in Figure 3. Apart from the final layer where softmax activation function [35] is employed for scores transformation into posterior probability at each node, RLU (rectified linear unit) activation function [36] is employed after the individual layer. In the convolutional layers, batch normalization [37] and the max-pooling over the dimension of frequency follow the activation function. Figures 4 (a, b) show the CNNs employed for separate estimation of θ and ϕ. Joint elevation and azimuth is possible by feeding the input of the CNN with SHM and SHP features with (θ, ϕ). Here, four possible techniques for the estimation of DoA are as follows.

1. NPSH-CNN: the normalized plain SH coefficients are employed for CNN training and joint (θ, ϕ) estimation.
2. SHP-CNN: SHP features are employed in the training of a CNN towards joint (θ, ϕ) estimation.
3. SHPM-CNN: SHPM features are employed for the training of a CNN towards joint (θ, ϕ) estimation.
4. SHP-SHPM-CNN: SHM and SHP features are used in the training of CNNs that corresponds to θ and ϕ, respectively.

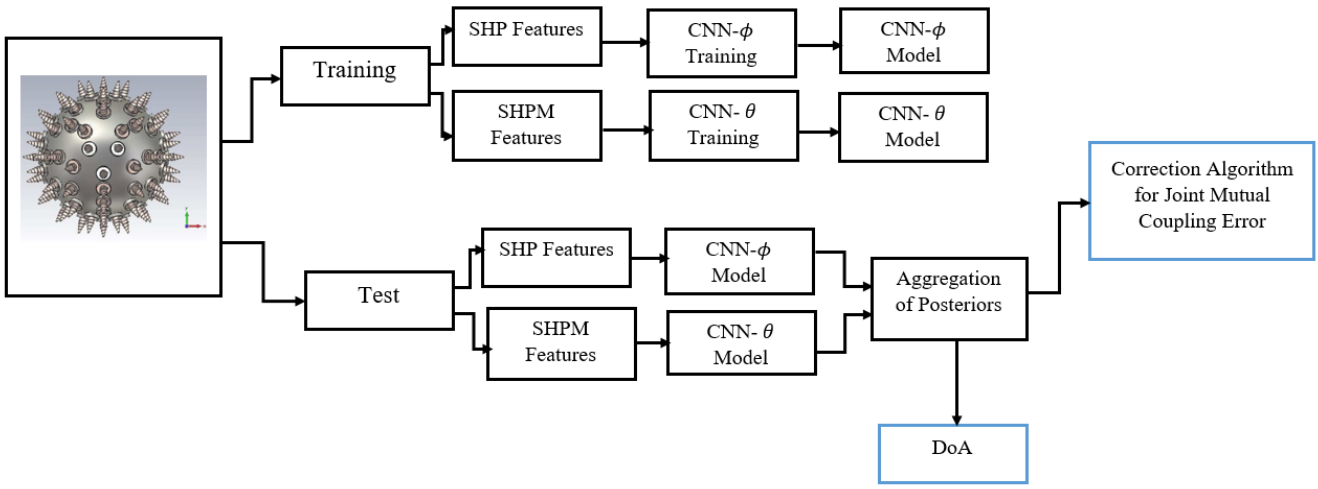

FIGURE 5. Proposed Procedure for DoA estimation and mutual coupling calibration.

C. COMPLEXITY OF TRAINING

The proposed method for estimation of DoA is not joint elevation and azimuth estimation. It becomes necessary to discuss the complexity issues in the training of the two methods. The complexity of sample defines the required number of training samples in the learning of mapping function, and it is a major training complexity parameter [38]. It is reported in the earlier evaluations [39] that to obtain the appropriate performance of a learning method, there should be at least a linear increase in the training samples with a number of parameters that can be trained [40]. In conventional CNN, the layers of FC provides up to 93 % of the whole parameters of the network [41]. Therefore, the complexity in training can be defined as a function of network parameters provided by the FC layers. The number of such parameters as observed from Figure 3 is $48\,(N_R - 3)\,N_H + N_H N_C$. Furthermore, the optimal N_H exists between the output layer and the size of the input [41]. For the DoA estimation proposed, $N_C = N_\theta + N_\phi$, the complexity of training becomes $O(N_R N_H + N_H(N_\theta + N_\phi))$. For the joint estimation using the similar architecture of the CNN in Figure 3, the complexity of training is $O(N_R N_H + N_H N_\theta N_\phi)$ for $N_C = N_\theta + N_\phi$ in joint estimation of DoA. For the developed DoA estimation, the resulted lower complexity in training allows the uncomplicated implementation of the proposed method even with a denser DoA search grid.

V. DOA CORRECTION ALGORITHM FOR JOINT MUTUAL COUPLING ERROR

The spatial smoothing algorithm has been proven to be an efficient method used to resolve the effects of the coherent source [42]. The basic idea is to divide the SAA into many overlapping subarrays [43]. By using the spectral function to search its maximum location, we can obtain the estimation of DoA of the signal. The coefficient of mutual coupling is estimated using the Lagrange method. For the sake of brevity and since the analysis is not our contribution to knowledge, readers are referred to [44] for the detailed analysis and explanation.

VI. THE PROPOSED SCHEME/ALGORITHM

The procedure of DoA estimation and mutual coupling calibration is as depicted in Figure 5. The DoA estimation is made up of two phases of training and testing, while the last stage holds the mutual coupling calibration. In the training phase, CNN-θ and CNN-ϕ are trained with SHPM and SHP features, respectively. The features are extracted and applying the trained model, the posterior probabilities, $\Pr(\theta|\zeta$ and $\Pr(\phi|\zeta$. The last stage is the DoA correction algorithm for joint mutual coupling error. This stage calibrates the mutual coupling. The whole process is as summarized in Algorithm 1. This algorithm uses the models and observations that are trained with SHPM and SHP features.

VII. EXPERIMENT

Although many papers deal with DoA and mutual coupling, only a few of them report experimental data, which are, in the end, the ground truth to test any procedure. Hence, real measurement data are used for analysis and performance evaluation in this paper.

A. MEASUREMENT

We acquired measurement data using an SAA [3] in an anechoic chamber. The SAA is stationed at the center of the chamber, and the source is located at 74 DoAs that are obtained from various combinations of 4 different elevations and 18 different azimuths. The azimuths are selected from 5^0 to 365^0 using a step size of 20^0. 85^0, 95^0, 105^0, 125^0 are the four elevations selected. The distance between the source and the SAA is maintained at 2 m. The mean time of measurements is almost 7 sec. Figure 6 depicts the experimental setup of the measurement for a stationary source for the estimation of DoA.

Algorithm 1 Proposed Algorithm for DoA Estimation and Mutual Coupling Calibration

Requirement: the observation matrix $\boldsymbol{p}(t)$ that contains the pressure of signal at all elements and the trained model that corresponds to SHP and SHPM features.

a: Calculate $\boldsymbol{p}(\rho, \varpi)$ by finding the STFT of $\boldsymbol{p}(t)$

b: Calculate $\boldsymbol{p}_{nm}(\rho, \varpi)$ via transformation of $\boldsymbol{p}(\rho, \varpi)$ to SH domain as $\boldsymbol{p}_{nm}(\rho, \varpi) = \boldsymbol{Y}^{H}(\Omega)\boldsymbol{p}(\rho, \varpi)$

c: Calculate $\boldsymbol{p}_{nm}(\rho, \varpi)$ by multiplying the left hand side with $\boldsymbol{B}^{-1}(kr)$ i.e. $\boldsymbol{p}_{nm}(\rho, \varpi) = \boldsymbol{B}^{-1}(kr)\boldsymbol{p}_{nm}(\rho, \varpi)$

d: Obtain the signal invariance via $q_{00}(\rho, \varpi)$ by

$$\angle\hat{q}(\rho, \varpi) = \angle q_{nm}(\rho, \varpi) - \angle q_{00}(\rho, \varpi)$$

e: Calculate SHP features as cosine and sine functions of

$$\angle\hat{q}_{nm}(\rho, \varpi)$$

f: Obtain the signal invariance via $q_{00}(\rho, \varpi)$ by

$$\left|\hat{q}_{nm}(\rho, \varpi)\right| = \left|q_{nm}(\rho, \varpi)\right| \Big/ \left|q_{00}(\rho, \varpi)\right|$$

g: Calculate SHM features via normalization of $\left|\hat{q}_{nm}(\rho, \varpi)\right|$

h: Obtain SHPM features by getting SHP and SHM features concatenated

i: Calculate $\Pr(\phi|\zeta)$ by feeding SHP as input into CNN-ϕ

j: Calculate $\Pr(\theta|\zeta)$ by feeding SHPM as input into CNN-θ

k: DoA estimation via MAP law as

$$\hat{\theta}_s = \arg\Pr(\theta|\zeta)$$
$$\hat{\phi}_s = \arg\Pr(\phi|\zeta)$$

l: For multiple frame, obtain DoA estimation by mean pooling of posteriors.

m: Apply DoA correction algorithm for joint mutual coupling error

B. TRAINING

For the training of CNN, Adam [45] is used as a stochastic optimization technique, while categorical cross-entropy serves as the loss function. The architectures of the CNN are trained using the corresponding datasets. 50% dropout and 20 epochs patience level is ensured for the avoidance of overfitting. Note, the behavior of the learning-based methods over the training and datasets were made similar; therefore, there was likely no overfitting. For the architectures and training sets, two DoA search grid resolutions are considered. (1) Sparse DoA search grid: SHPM-CNN, SHP-CNN and SHP-SHPM-CNN are trained. (2) Dense DoA search grid: we only considered SHP-SHPM-CNN due to the complexity in training.

C. PERFORMANCE EVALUATION

It was identified in the literature that RMSE (root mean square error) could cause outliers, another robust measure that is not affected by outliers is presented in this paper. Similar performance metrics have already been used in [46]–[48]. GE (gross error) is a percentage estimate, which does not fall

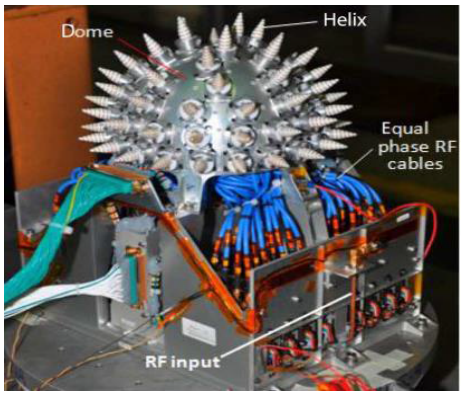

(a)

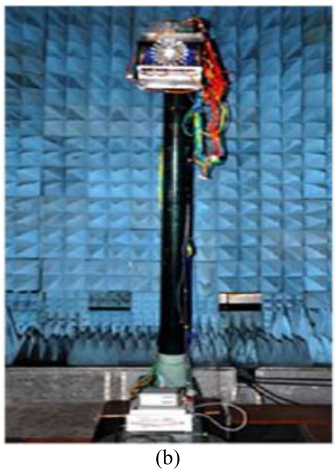
(b)

FIGURE 6. Experimental setup for measurement using SAA. (a) SAA (b) Configuration of the SPAA in anechoic chamber.

to a permitted level from the correct value. The measure of GE is expressed as

$$GE = \frac{1}{N_T}\sum_{j=1}^{N_T}\left[I_e\left(\Delta\left((\theta, \phi), \left(\hat{\theta}, \hat{\phi}\right)\right) - \lambda\right)\right]$$
$$GE_{\phi} = \frac{1}{N_T}\sum_{j=1}^{N_T}\left[I_e\left(\left|\phi_j - \hat{\phi}_j\right| - \lambda\right)\right]$$
$$GE_{\theta} = \frac{1}{N_T}\sum_{j=1}^{N_T}\left[I_e\left(\left|\theta_j - \hat{\theta}_j\right| - \lambda\right)\right] \quad (27)$$

where N_T is the total number of estimated DoAs, $(\theta_j - \phi_j)$ and $(\hat{\theta}_j - \hat{\phi}_j)$ are real and the estimated DoAs of the jth sample, respectively. Δ defines the angular distance based on cosine similarity as

$$\Delta\left((\theta, \phi), \left(\hat{\theta}, \hat{\phi}\right)\right) = \arccos\left(sin\hat{\theta}sin\theta + cos\hat{\theta}cos\theta\cos\left(\hat{\phi} - \phi\right)\right).$$

I_e represents indicator function expressed as

$$I_e(x) = \begin{cases} 0 & for\ x < 0 \\ 1 & for\ x \geq 0 \end{cases} \quad (28)$$

TABLE 1. Average gross error of different methods over a sparse DoA search grid. λs are in degrees.

	SH-MUSIC [8]		SH-MUSIC-DPD [51], [52]		PSH-CNN		SHP-CNN		SHPM-CNN		SHP-SHPM-CNN	
N_B	$\lambda = 10^0$	$\lambda = 20^0$	$\lambda = 10^0$	$\lambda = 20^0$	$\lambda = 10^0$	$\lambda = 20^0$	$\lambda = 10^0$	$\lambda = 20^0$	$\lambda = 10^0$	$\lambda = 20^0$	$\lambda = 10^0$	$\lambda = 20^0$
20	87.90	73.92	52.73	44.50	39.98	32.95	28.18	24.36	32.35	27.83	34.78	27.04
60	83.99	66.72	31.65	22.28	17.41	12.90	8.99	6.65	12.90	10.47	12.55	8.73
100	81.65	66.37	16.37	10.42	8.73	6.91	4.57	4.22	6.30	5.26	7.35	5.26

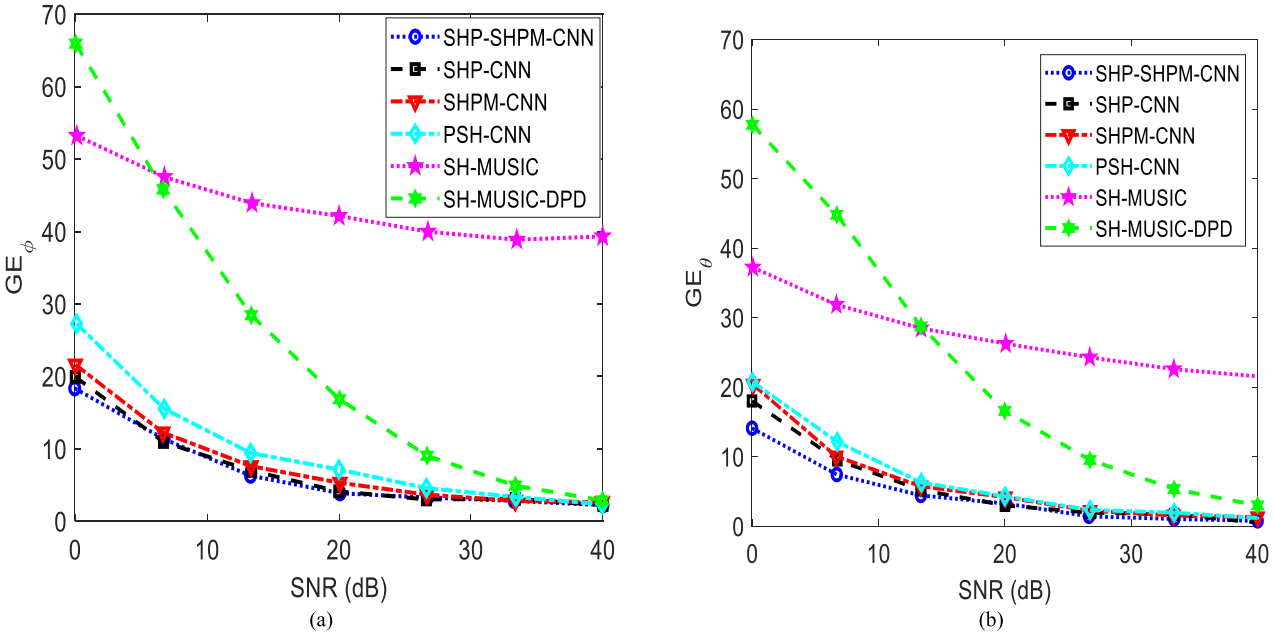

FIGURE 7. Performance evaluation of methods over a sparse DoA search grid. (a) GE_ϕ versus SNR and (b) GE_θ versus SNR for $N_B = 100$ and $\lambda = 20^0$.

TABLE 2. Average gross error of different methods over a Dense DoA search grid. λs are in degrees.

	SH-MUSIC-DPD			SHP-SHPM-CNN		
N_B	$\lambda = 5^0$	$\lambda = 10^0$	$\lambda = 20^0$	$\lambda = 5^0$	$\lambda = 10^0$	$\lambda = 20^0$
20	76.00	55.26	44.15	58.99	37.56	28.18
60	61.16	33.39	21.93	31.91	13.25	8.99
100	52.83	20.19	10.12	20.19	5.96	4.91

D. GE ANALYSIS OF SPARSE DoA SEARCH GRID

The comparison of the performance of different methods over a sparse DoA search grid for various λ and N_B is presented in Table 1. The results presented are averaged over various SNRs in the test dataset. The performance of different methods for various SNR is as shown in Figure 7. $N_B = 100$ and $\lambda = 20^0$ are used for GE_ϕ and GE_θ.

Based on the experiments over a sparse DoA search grid, the proposed methods perform better than previous methods. SH-MUSIC-DPD performs better than SH-MUSIC under all conditions of λ and N_B when averaged over SNR. The SH-MUSIC-DPD outperforms SH-MUSIC between 5 and 10 dB SNR in both GE_ϕ and GE_θ. The newly developed methods: SHP-CNN, SHPM-CNN and SHP-SHPM-CNN perform better than PSH-CNN for all cases. This is due to the associated feature extraction in our proposed methods. All the above observations are so because neural networks exhibit a high level of robustness against noise [16].

E. GE ANALYSIS OVER A DENSE DoA SEARCH GRID

The results obtained from the previous and the proposed methods for estimation of DoA over a denser grid are presented in Table 2. The GE for $N_B = 100$ and $\lambda = 5^0, 10^0$ versus SNR is presented in Figure 8. It can be observed that the proposed method performs better than other methods. The proposed method resolves 40% of signals within the threshold of 5^0 and $N_B = 20$. The GE observed with $\lambda = 10^0 and 20^0$ for dense DoA search grid share similar characteristics with that of sparse DoA search grid achieved. In addition,

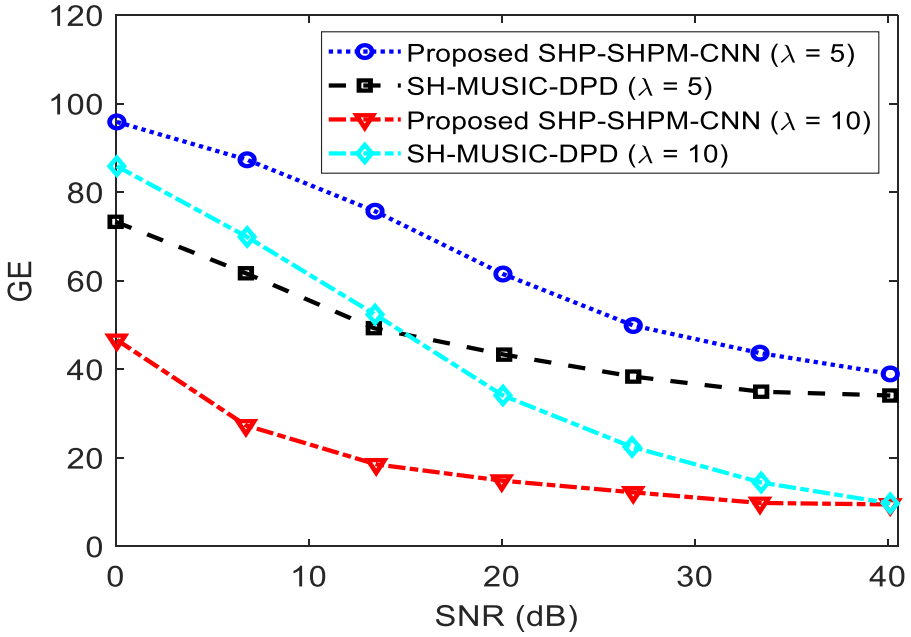

FIGURE 8. Performance evaluation of methods over a dense DoA search grid using GE versus SNR for $N_B = 100$ and $\lambda = 5^0, 10^0$.

TABLE 3. The elapsed time for each signal for estimation of DoA for different DoA search grid resolution and N_B. Simplies search while D implies dense.

	SH-MUSIC-DPD		SHP-SHPM-CNN	
N_B	S (s)	D (s)	S (s)	D (s)
20	0.17	0.39	0.10	0.18
60	0.26	0.54	0.21	0.23
100	0.85	1.36	0.41	0.45

the proposed method shows more robustness against noise compared to other methods.

F. COMPLEXITY ANALYSIS

We experimented with the run-time complexity comparison of SHP-SHPM-CNN with that of the SH-MUSIC-DPD. Note that there is non-parallel processing for the implementation of the two methods. Matlab was used to execute the two methods. A computer system with core i7, 8th Gen., Intel processor, 16 GB RAM, 1T hard-drive, and 64-bit instruction set is used to execute the algorithms. Signals from the test dataset are employed for estimating the elapsed time for both methods. The comparison of the average elapsed time for varying N_B and dense/sparse DoA search grid is presented in Table 3. It is observed that an increase in the DoA search grid resolution impairs SH-MUSIC-DPD more than the proposed method. The proposed method provides an appreciable fall in computational complexity. The proposed method exhibits better performance and reduced computational complexity.

G. MUTUAL COUPLING CALIBRATION

With the recent advancement in baseband integrated circuits and radio frequency (RF) technology, there is a strong demand to minimize the size of array-based microwave systems. However, array aperture miniaturization often leads to strong mutual coupling in the arrays. To date, mitigating or compensating the mutual coupling (nonlinear) effect remains a technical challenge. In this section, we compared the proposed method with the spatial smoothing algorithm [49]. Using the same setup in Section VI, the noise is zero-mean Gaussian white noise. Considering two signal sources having 0 and 70 azimuth degrees, and setting the SNR at 10 dB. It is depicted in Figure 9 how spatial smoothing algorithm did not obtain an appropriate spectral peak due to mutual coupling, while the proposed method correctly obtain the direction of the wave. Figure 10 shows that the uncoupling joint estimation algorithm is unable to identify source direction.

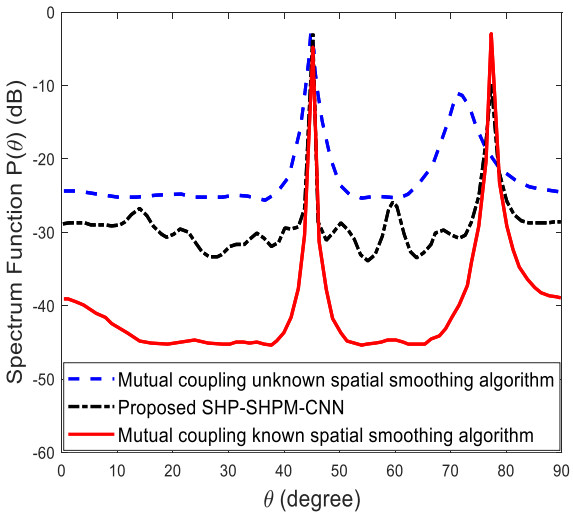

FIGURE 9. Spatial spectrum profile.

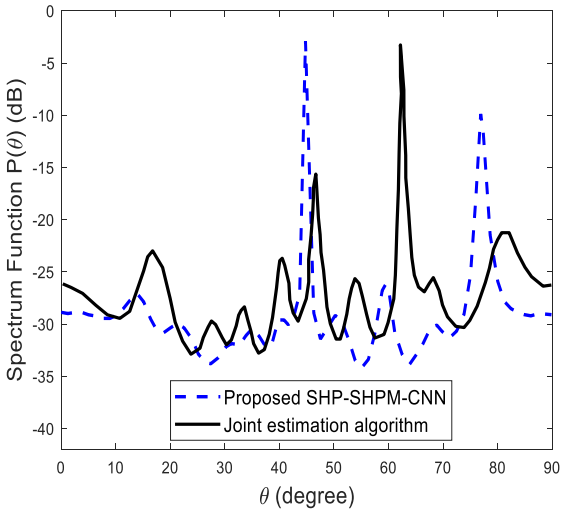

FIGURE 10. Spatial spectrum comparison.

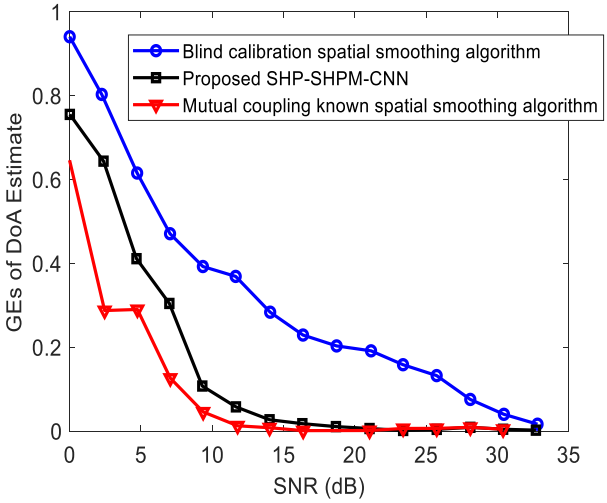

FIGURE 11. GEs of DoA estimate against SNR.

The joint estimation algorithm exhibits large errors and fails in multipath scenario. The proposed method can get accurate spectrum peak in the multipath scenario with unknown mutual coupling, with sharper spectrum peak.

Comparing the appropriateness of the proposed method, with the blind calibration spatial smoothing algorithm and mutual coupling known spatial smoothing algorithm [49]. Figure 11 indicates the GE comparison of individual DoA estimate under different SNRs with 200 snapshots. The GEs of DoA estimate for different snapshots are as shown in Figure 12. As observed from Figure 11, all the exhibits a downward profile and approach zero as SNR increases, and the proposed method's accuracy is higher than the blind calibration space smoothing algorithm [49]. Figure 12 shows that the accuracy of the angle measurement of all the methods gives better performance and more correct as the snapshots increases. As the snapshot numbers become bigger than 130,

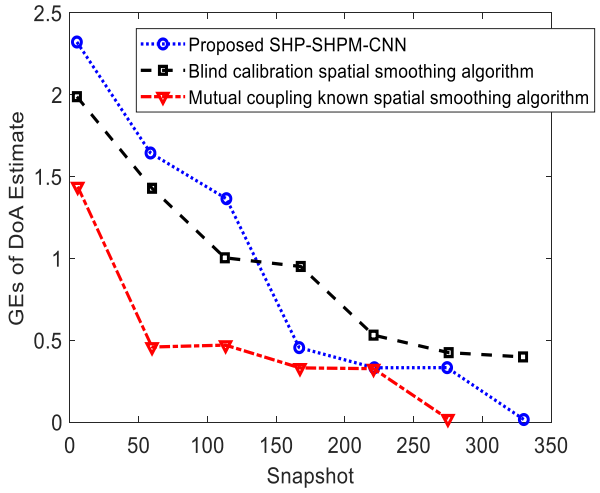

FIGURE 12. GEs of DoA estimate against snapshot.

the proposed method exhibits better angle measurement accuracy than the blind calibration space smoothing algorithm.

VIII. CONCLUSION

In conclusion, this paper presents a robust DoA estimation and mutual coupling compensation technique based on convolutional neural network (CNN) for Spherical Array. SHD has been used to facilitate feature extraction in two sets that contain different features about the elevation and azimuth of the source for DoA estimation. The features serve as input to the learning technique for separate estimation of elevation and azimuth. Learning methods for DoA estimation with few frames and dense search grids within the spherical array configuration is also developed. In addition to the proposed DoA estimation algorithm, a mutual coupling calibration is adapted. The mutual coupling is based on special MCM structure and spatial smoothing algorithms. There is an appreciable improvement in the estimation of DoA, even in a harsh environment. The proposed method exhibits better performance and reduced computational complexity. Also, it exhibits noticeable performance in the mitigation of mutual coupling in SAA. In addition, The experimental results, which is the ground truth to test any procedure, show the validity and potential practical application of the proposed method. This method may spur positive development in other areas and related applications, such as angle-of-arrival (AoA) estimation and time-delay measurements.

REFERENCES

[1] M. Carlin, P. Rocca, G. Oliveri, F. Viani, and A. Massa, "Directions-of-arrival estimation through Bayesian compressive sensing strategies," *IEEE Trans. Antennas Propag.*, vol. 61, no. 7, pp. 3828–3838, Jul. 2013.

[2] M. G. Pralon, G. Del Galdo, M. Landmann, M. A. Hein, and R. S. Thoma, "Suitability of compact antenna arrays for direction-of-arrival estimation," *IEEE Trans. Antennas Propag.*, vol. 65, no. 12, pp. 7244–7256, Dec. 2017.

[3] B. P. Kumar, C. Kumar, V. S. Kumar, and V. V. Srinivasan, "Active spherical phased array design for satellite payload data transmission," *IEEE Trans. Antennas Propag.*, vol. 63, no. 11, pp. 4783–4791, Nov. 2015.

[4] M. A. Preston and J. P. Lyons, "A switched reluctance motor model with mutual coupling and multi-phase excitation," *IEEE Trans. Magn.*, vol. 27, no. 6, pp. 5423–5426, Nov. 1991.

[5] W. Ding, D. Liang, and H. Sui, "Dynamic modeling and performance prediction for dual-channel switched reluctance machine considering mutual coupling," *IEEE Trans. Magn.*, vol. 46, no. 9, pp. 3652–3663, Sep. 2010.
[6] C. Kumar, B. P. Kumar, V. S. Kumar, and V. V. Srinivasan, "Dual circularly polarized spherical phased-array antenna for spacecraft application," *IEEE Trans. Antennas Propag.*, vol. 61, no. 2, pp. 598–605, Feb. 2013.
[7] V. Y. Vu, A. J. Braga, X. Begaud, and B. Huyart, "Measurement of direction-of-arrival of coherent signals using five-port reflectometers and quasi-Yagi antennas," *IEEE Microw. Wireless Compon. Lett.*, vol. 15, no. 9, pp. 558–560, Sep. 2005.
[8] L. Kumar, G. Bi, and R. M. Hegde, "The spherical harmonics root-music," in *Proc. IEEE Int. Conf. Acoust., Speech Signal Process. (ICASSP)*, Mar. 2016, pp. 3046–3050.
[9] H. Sun, E. Mabande, K. Kowalczyk, and W. Kellermann, "Joint DOA and TDOA estimation for 3D localization of reflective surfaces using eigenbeam MVDR and spherical microphone arrays," in *Proc. IEEE Int. Conf. Acoust., Speech Signal Process. (ICASSP)*, May 2011, pp. 113–116.
[10] E. Mabande, H. Sun, K. Kowalczyk, and W. Kellermann, "Comparison of subspace-based and steered beamformer-based reflection localization methods," in *Proc. Eur. Signal Process. Conf.*, Aug. 2011, pp. 146–150.
[11] S. Adavanne, A. Politis, and T. Virtanen, "Direction of arrival estimation for multiple sound sources using convolutional recurrent neural network," in *Proc. 26th Eur. Signal Process. Conf.*, Sep. 2018, pp. 1462–1466.
[12] B. Laufer-Goldshtein, R. Talmon, and S. Gannot, "Semi-supervised sound source localization based on manifold regularization," *IEEE/ACM Trans. Audio, Speech, Lang. Process.*, vol. 24, no. 8, pp. 1393–1407, Aug. 2016.
[13] S. Chakrabarty and E. A. P. Habets, "Broadband DOA estimation using convolutional neural networks trained with noise signals," in *Proc. IEEE Workshop Appl. Signal Process. Audio Acoust.*, Oct. 2017, pp. 136–140.
[14] R. Takeda and K. Komatani, "Sound source localization based on deep neural networks with directional activate function exploiting phase information," in *Proc. IEEE Int. Conf. Acoust., Speech Signal Process.*, Mar. 2016, pp. 405–409.
[15] R. Takeda and K. Komatani, "Discriminative multiple sound source localization based on deep neural networks using independent location model," in *Proc. IEEE Spoken Lang. Technol. Workshop (SLT)*, Dec. 2016, pp. 603–609.
[16] X. Xiao, S. Zhao, X. Zhong, D. L. Jones, E. S. Chng, and H. Li, "A learning-based approach to direction of arrival estimation in noisy and reverberant environments," in *Proc. IEEE Int. Conf. Acoust., Speech Signal Process. (ICASSP)*, Apr. 2015, pp. 2814–2818.
[17] F. Vesperini, P. Vecchiotti, E. Principi, S. Squartini, and F. Piazza, "A neural network based algorithm for speaker localization in a multi-room environment," in *Proc. IEEE 26th Int. Workshop Mach. Learn. Signal Process. (MLSP)*, Sep. 2016, pp. 1–6.
[18] S. Chakrabarty and E. A. P. Habets, "Broadband DOA estimation using convolutional neural networks trained with noise signals," 2017, *arXiv:1705.00919*. [Online]. Available: http://arxiv.org/abs/1705.00919
[19] S. Adavanne, A. Politis, and T. Virtanen, "Direction of arrival estimation for multiple sound sources using convolutional recurrent neural network," 2017, *arXiv:1710.10059*. [Online]. Available: http://arxiv.org/abs/1710.10059
[20] Z.-M. Liu, C. Zheng, and P. S. Yu, "Direction-of-arrival estimation based on deep neural networks with robustness to array imperfection," *IEEE Trans. Antennas Propag.*, vol. 66, no. 12, pp. 7315–7328, Dec. 2018.
[21] Y. Kase, T. Nishimura, T. Ohgane, Y. Ogawa, D. Kitayama, and Y. Kishiyama, "DOA estimation of two targets with deep learning," in *Proc. 15th Workshop Positioning, Navigat. Commun. (WPNC)*, Bremen, Germany, Oct. 2018, pp. 1–5.
[22] L. Wan, Y. Sun, L. Sun, Z. Ning, and J. J. P. C. Rodrigues, "Deep learning based autonomous vehicle super resolution DOA estimation for safety driving," *IEEE Trans. Intell. Transp. Syst.*, early access, Aug. 21, 2020, doi: 10.1109/TITS.2020.3009223.
[23] F. Wen, J. Wang, J. Shi, and G. Gui, "Auxiliary vehicle positioning based on robust DOA estimation with unknown mutual coupling," *IEEE Internet Things J.*, vol. 7, no. 6, pp. 5521–5532, Jun. 2020.
[24] A. M. Elbir, "A novel data transformation approach for DOA estimation with 3-D antenna arrays in the presence of mutual coupling," *IEEE Antennas Propag. Lett.*, vol. 16, pp. 2118–2122, Apr. 2017.
[25] T. Zhang and W. Ser, "Robust beampattern synthesis for antenna arrays with mutual coupling effect," *IEEE Trans. Antennas Propag.*, vol. 59, no. 8, pp. 2889–2895, Aug. 2011.
[26] H. Aoyama, "Mutual coupling matrix estimation and null forming methods for MBF antennas," *IEICE Trans. Commun.*, vol. E88-B, no. 6, pp. 2305–2312, Jun. 2005.
[27] Y. Wu, G. Liao, and H. C. So, "A fast algorithm for 2-D direction-of-arrival estimation," *Signal Process.*, vol. 83, no. 8, pp. 1827–1831, Aug. 2003.
[28] N. Tayem and H. M. Kwon, "Azimuth and elevation angle estimation with no failure and no eigen decomposition," *Signal Process.*, vol. 86, no. 1, pp. 8–16, Jan. 2006.
[29] N. Xi and L. Liping, "A computationally efficient subspace algorithm for 2-D DOA estimation with L-shaped array," *IEEE Signal Process. Lett.*, vol. 21, no. 8, pp. 971–974, Aug. 2014.
[30] B. Rafaely, *Fundamentals of Spherical Array Processing*, vol. 8. Berlin, Germany: Springer, 2015.
[31] B. G. B. Arfken and H. J. Weber, *Mathematical Methods for Physicists*. New York, NY, USA: Elsevier, 1999.
[32] B. Rafaely, "Analysis and design of spherical microphone arrays," *IEEE Trans. Speech Audio Process.*, vol. 13, no. 1, pp. 135–143, Jan. 2005.
[33] V. Varanasi and R. Hegde, "Robust online direction of arrival estimation using low dimensional spherical harmonic features," in *Proc. IEEE Int. Conf. Acoust., Speech Signal Process.*, Mar. 2017, pp. 511–515.
[34] B. M. P. J. Braspenning, F. Thuijsman, and A. J. M. M. Weijters, *Artificial Neural Networks: An Introduction to ANN Theory and Practice*, vol. 931. Berlin, Germany: Springer, 1995.
[35] A. Krizhevsky, I. Sutskever, and G. E. Hinton, "ImageNet classification with deep convolutional neural networks," in *Proc. Adv. Neural Inf. Process. Syst.*, 2012, pp. 1097–1105.
[36] C. M. Bishop, *Neural Networks for Pattern Recognition*. London, U.K.: Oxford Univ. Press, 1995.
[37] S. Ioffe and C. Szegedy, "Batch normalization: Accelerating deep network training by reducing internal covariate shift," in *Proc. Int. Conf. Mach. Learn.*, vol. 37, 2015, pp. 448–456.
[38] B. M. R. Livni, S. Shalev-Shwartz, and O. Shamir, "On the computational efficiency of training neural networks," in *Proc. Adv. Neural Inf. Process. Syst.*, 2014, pp. 855–863.
[39] P. L. Bartlett, "The sample complexity of pattern classification with neural networks: The size of the weights is more important than the size of the network," *IEEE Trans. Inf. Theory*, vol. 44, no. 2, pp. 525–536, Mar. 1998.
[40] Y. Cheng, F. X. Yu, R. S. Feris, S. Kumar, A. Choudhary, and S.-F. Chang, "An exploration of parameter redundancy in deep networks with circulant projections," in *Proc. IEEE Int. Conf. Comput. Vis.*, Dec. 2015, pp. 2857–2865.
[41] J. Heaton, *Introduction to Neural Networks With Java*. St. Louis, MO, USA: Heaton Research, 2008.
[42] A. Das, W. S. Hodgkiss, and P. Gerstoft, "Coherent multipath direction-of-arrival resolution using compressed sensing," *IEEE J. Ocean. Eng.*, vol. 42, no. 2, pp. 494–505, Apr. 2017.
[43] T. Filik and T. E. Tuncer, "2-D DOA estimation in case of unknown mutual coupling for multipath signals," *Multidimensional Syst. Signal Process.*, vol. 27, no. 1, pp. 69–86, Jan. 2016.
[44] L. Qin, C. Li, Y. Du, and B. Li, "DoA estimation and mutual coupling calibration algorithm for array in plasma environment," *IEEE Trans. Plasma Sci.*, vol. 48, no. 6, pp. 2075–2083, Jun. 2020.
[45] D. P. Kingma and J. Ba, "Adam: A method for stochastic optimization," in *Proc. Int. Conf. Learn. Represent.*, 2015, pp. 1–15.
[46] B. M. S. Brandstein and H. F. Silverman, "A robust method for speech signal time-delay estimation in reverberant rooms," in *Proc. IEEE Int. Conf. Acoust., Speech, Signal Process.*, Apr. 1997, vol. 1, pp. 375–378.
[47] F. Athley, "Performance analysis of DOA estimation in the threshold region," in *Proc. IEEE Int. Conf. Acoust. Speech Signal Process.*, vol. 3, May 2002, pp. 3017–3020.
[48] L. Kumar and R. M. Hegde, "Near-field acoustic source localization and beamforming in spherical harmonics domain," *IEEE Trans. Signal Process.*, vol. 64, no. 13, pp. 3351–3361, Jul. 2016.
[49] J. Dai and Z. Ye, "Spatial smoothing for direction of arrival estimation of coherent signals in the presence of unknown mutual coupling," *IET Signal Process.*, vol. 5, no. 4, pp. 418–425, Jul. 2011.
[50] O. Nadiri and B. Rafaely, "Localization of multiple speakers under high reverberation using a spherical microphone array and the direct-path dominance test," *IEEE/ACM Trans. Audio, Speech, Language Process.*, vol. 22, no. 10, pp. 1494–1505, Oct. 2014.
[51] B. Rafaely and D. Kolossa, "Speaker localization in reverberant rooms based on direct path dominance test statistics," in *Proc. IEEE Int. Conf. Acoust., Speech Signal Process.*, Mar. 2017, pp. 6120–6124.

OLUWOLE JOHN FAMORIJI (Member, IEEE) received the B.Tech. degree in electrical and electronic engineering from the Ladoke Akintola University of Technology, Ogbomoso, Nigeria, in 2009, the M.Eng. degree in communications engineering from the Federal University of Technology Akure, Akure, Nigeria, in 2014, and the Ph.D. degree in electronic science and technology from the University of Science and Technology of China (USTC), Hefei, China, in 2019. He is currently a Research Fellow with Zhejiang University. His research interests include signals and systems, array processing, and antenna and propagation. He was a recipient of one of the Best Papers and Oral Presentation Award of the 2018 IEEE International Conference on Integrated Circuits and Technology Applications (ICTA), Beijing. He also received the 2016 Innovation Spirit Award of the Micro-/Nano-Electronics System Integration Center and Institute of Microelectronics Electronics Chinese Academy of Science (MESIC-IMECAS).

OLUDARE Y. OGUNDEPO received the B.S. degree from the Faculty of Engineering, Ladoke Akintola University of Technology, Ogbomoso, Nigeria, in 2009, the M.E. degree from the Federal University of Technology Akure, Nigeria, in 2014, and the Ph.D. degree in communication engineering from the University of Ilorin, Nigeria. His current research interests include RF theory, navigation algorithm, and array signal processing.

XIAOKANG QI (Member, IEEE) received the B.S. degree from the School of Electronics and Information, Northwestern Polytechnical University, Xi'an, China, in 2013, and the Ph.D. degree from the College of Information Science and Electronics Engineering, Zhejiang University, Hangzhou, China, in 2018. His current research interests include RF theory, navigation algorithm, and sensor systems.